



Simulation of two-phase flow and mass transfer of CO₂ bubbles in a sweetener solution by horizontal pipe using Comsol

Ahmed Dheyaa Nsaif ^{a,*}, Ibtihal Kareem Shakir ^a, Munaf Al-Lami ^b

^a Department of Chemical Engineering, College of Engineering, University of Baghdad, Baghdad, Iraq

^b Department of Chemical and Environmental Process Engineering, Faculty of Chemical Technology and Biotechnology, Budapest University of Technology and Economics, H-1111 Budapest, Hungary

Abstract

This research investigated the two-phase flow behavior and mass transfer of CO₂ bubbles in a water-sucrose solution in a horizontal pipe. The process used A Computational Fluid Dynamic (CFD) model that offers diverse applications in numerous industries. The simulation of two-phase flow with mass transfer is carried out using COMSOL[®] software version 5.6 and compared with experimental results. The model verified satisfactory concurrence with the experimental data. Multivariable such as concentration, velocity, and share rate were studied under different conditions (gas flow rate, liquid flow rate, bubble diameter, pipe diameter, and sucrose concentration). The gas flow rate was varied at the inlet, with values of (0.2, 0.45, and 0.7 L/min) for CO₂ and (2, 4, and 6 L/min) for the sweeteners solution. The diameter of the bubbles ranged from (2 to 4 mm). The pipe diameter was (1.25 and 1.9 cm), and the sucrose concentration in the sweetener solution was (150 g/L). It was observed that the effect of bubble diameter was inversely to CO₂ concentration, and the gas and liquid flow rates were directly proportional to concentration. The concentration of CO₂ decreases as the concentration of sucrose increases. The relationship between bubble diameter and gas phase velocity was inverse, as well as studying the effect of variables on share rate.

Keywords: Two-phase Flow; COMSOL CFD; mass Transfer; CO₂ bubbles; Horizontal pipe.

Received on 21/01/2024, Received in Revised Form on 13/07/2024, Accepted on 13/07/2024, Published on 30/03/2025

<https://doi.org/10.31699/IJCPE.2025.1.5>

1- Introduction

The soft drink industry is considered one of the most widespread industries in the world. It involves a large percentage of water along with other materials such as sugar, carbon dioxide, and other additives according to the permitted percentages [1].

Therefore, it is necessary to study the influence of operational conditions and geometric variables on the mass and heat transfer of the two-phase flow of CO₂ bubbles with sweetener solutions in a horizontal tube to reduce production time and costs. Despite their importance in industry, the literature has paid less attention to horizontal bubbly flow than vertical flows [2]. The two-phase flow phenomena manifested in several forms, such as the counter flow of gas and liquid, the presence of two liquid phases, and a mixture of liquid and solid particles. While it is a relatively straightforward approach to modify the design's parameters in a single phase, understanding the dynamics of two-phase fluid flow has shown preeminent difficulties due to its inherent complexity and demanding behavior [3].

Modern technology has offered straightforward and uncomplicated answers through mathematical models to confront the challenges associated with comprehending two-phase flow and to facilitate these complexities for researchers [4, 5].

CFD model applying mechanics principles to fluids that yield associated non-linear partial differential equations. Engineering typically solves these equations analytically. The conservation of matter, momentum, and energy in a fluid's region of interest is considered while creating mathematical models. Simplifying assumptions for proper initial and boundary conditions are required to solve the problem effortlessly. Initial and boundary conditions are necessary to solve the Navier-Stokes and the continuity equation [6]. Several mathematical models were used to represent a two-phase flow, depending on the required boundary conditions, and the flow type (laminar or turbulent). The flow is distinguished by bubble flow, mixture flow model, and Euler-Euler model [7].

Flow patterns can disperse phases differently in a two-phase liquid-gas flow. Identifying the flow pattern is significant for determining crucial variables such as liquid hold-up and pressure drop. In horizontal flow, gravity acts perpendicular to the axial direction, which can cause phase separation. The four primary flow patterns in horizontal flow are bubbly, stratified, slug, and annular. In bubbly flow, the gas phase distributed bubbles inside the continuous liquid phase. A stratified flow has a smooth liquid-gas interface with no droplet entrainment in the gas phase that travels above the liquid phase [8]. This simulation used a bubble flow model with mass transfer.



*Corresponding Author: Email: ahmed.nasif1507d@coeng.uobaghdad.edu.iq

© 2025 The Author(s). Published by College of Engineering, University of Baghdad.

This is an Open Access article licensed under a [Creative Commons Attribution 4.0 International License](https://creativecommons.org/licenses/by/4.0/). This permits users to copy, redistribute, remix, transmit and adapt the work provided the original work and source is appropriately cited.

Simulation systems predict experimental results, as it is simple to change operational conditions and the type of materials used during the simulation process.

CO₂ gas flow in a near horizontal pipe has been simulated and compared with the experimental results. It found that a multi-mixture modelling concept is the most appropriate model. Generally, the CO₂ behavior of two-phase flow in a near horizontal pipe represents a combination of the traditional two-fluid and the drift-flux models. This model effectively predicted CO₂ two-phase flows in a near-horizontal pipe, as presented by simulation data. The models accurately predicted flow regime transition, pressure gradient, and liquid holdup in a near-horizontal pipe for CO₂ two-phase flow [8].

The two-phase flow development followed investigation and experimental observation of an expansion device. It is directed at optimizing a vertical flash tank separator. Following the expansion device, an experimental apparatus was constructed to provide the necessary operating conditions for the two-phase flow production. The two-phase flow was evaluated by simulating it using the CFD [9].

A methodology has been developed to determine the flow regime using dynamic pressure signals and deep learning techniques. Laminar, slug, and annular flow regimes were simulated using the Level-Set (LS) method combined with the Volume of Fluid (VOF) method in a 6 m long horizontal tube with an inner diameter of 0.050 m. Strategically located dynamic pressure signals were collected. Deep learning architectures like ResNet50 and Shuffle Net employed scalograms of these signals. Both architectures classified flow regimes with 85.7% and 82.9% accuracy, respectively [10].

A comprehensive computational fluid dynamic model was developed for comparison with the experimental results presented by Kocamustafaogullari and Wang [11], Kocamustafaogullari and Huang [12], and Iskandrani and Kojasoy [13]. Two models, k- ϵ with constant bubble size and k- ϵ with population balance model, indicate excellent quantitative agreement with experimental results for a wide range of superficial gas and liquid velocities (0.2-1.0 m/s and 3.8-5.1 m/s, respectively). As the population balance was determined, the model prediction showed superior concordance with the experimental data compared to the prediction specified on constant bubble diameter [14].

In this work, the simulation was programmed based on multiphase Turbulent bubbly flow k- ω turbulence models and chemical transport of dilute species in two solutions (RO water, RO water +150 g/l sucrose) by using COMSOL Multiphysics based on the Finite Element Method to determine an approximate solution for the relevant Partial Differential Equations that describes the system. The influence of the parameters on CO₂ concentration distribution, share rate, and gas phase velocity was studied, such as gas flow rate (0.2, 0.45, and 0.7 L/min), liquid flow rate (2.4 and 6 L/min), bubble diameter (0.002 and 0.004m), pipe diameter (1.25 and 1.9 cm), and sucrose concentration. Lastly, the simulation

data was compared with the collected experimental results.

2- Experimental methods

Fig. 1 illustrates the lab scale process flow diagram (PFD) for the two-phase flow horizontal pipe CO₂-sweetener solution of the steady-state absorption System. The experimental equipment consisted of a horizontal pipe, two mass flow controllers (Brooks 5851i and Sam Fantas SFC1480FAPD2PL8) to determine the gas injection and measure the undissolved gas flow rate, two booster pumps to circulate sweetener solution, a gas separator to separate gas from liquid, a sweetener solution isolated storage tank with a refrigeration temperature controller system to make the temperature of the solution constant, a stainless steel gas diffuser to determine the starting size of the bubble, and a power supplies to run the operation and setting the mass flow controller. The solvents employed in this experiment were (RO water) and (RO water +150 g/L sucrose).

A refrigeration temperature control system initially maintained the system's temperature at a steady 20 °C. The pumps then initiated the circulation of the solution from the isolated storage tank and horizontal pipe (1.25 and 1.9 cm) to the separator. When the water level within the separator became stable, the CO₂ inlet flow rate was (0.2, 0.45, and 0.7 L/min) and the sweetener solution flow rate was (2.4 and 6 L/min). A mixture of water and carbon dioxide was introduced into the separator by the horizontal pipe. Once inside, the mixture was separated into the dissolved and undissolved gas. The mass flow controller was used to determine the precise quantity of gas that had not been dissolved. For the experimental variables and levels, Table 1 presents a definition.

Table 1. Variables and levels

Parameter	Units	Levels		
Gas flow rate	L/min	0.2	0.45	0.7
Liquid flow rate	L/min	2	4	6
Bubble diameter	m	0.002		0.004
Pipe diameter	cm	1.25		1.9
Sucrose concentration	g/L	0		150
Temperature	°C		20	

According to the equation that follows, the rate of solution can be determined.

$$\dot{m} = \dot{m}_{\text{injected}} - \dot{m}_{\text{residual}} \quad (1)$$

$\dot{m}_{\text{injected}}$ and $\dot{m}_{\text{residual}}$ are the injected and undissolved gases, respectively. The MFC measures the rate of undissolved residual gas and input gas. The difference between these numbers is the gas dissolution rate [15].

$$k = \frac{\dot{m}}{\pi d_b^2 (C^* - C^L)} \quad (2)$$

Where \dot{m} is the dissolving rate from Eq. 1 experiments, and d_b^2 is the bubble diameter. C^* is the saturation concentration of the gas, and C^L is a solute-dissolved concentration. Table 2 shows the Experimental Run and Results, the rate of solution, mass transfer coefficient, and CO₂ concentration at 20 °C.

Table 2. Experimental run and results

Run No.	gas rate L/min	flow rate L/min	liquid flow rate L/min	Bubble diameter m	Concentration g/L	pipe diameter m	Rate transfer g/min	mass CO ₂ g/m ³	Concentration K
1	0.7	2	0.002	0	0.01905	0.71	8.07	0.0032	
2	0.2	6	0.002	0	0.0127	0.37	1.4	0.0298	
3	0.2	2	0.002	0	0.0127	0.28	3.18	0.008	
4	0.2	6	0.004	0	0.0127	0.31	1.17	0.0499	
5	0.45	4	0.004	0	0.0127	0.72	4.09	0.037	
6	0.7	6	0.004	0	0.0127	1.11	4.2	0.0552	
7	0.2	2	0.002	0	0.01905	0.14	1.59	0.0018	
8	0.7	6	0.002	0	0.01905	1.1	4.17	0.0121	
9	0.45	4	0.002	0	0.01905	0.58	3.3	0.0066	
10	0.7	2	0.004	0	0.01905	0.66	7.5	0.0059	
11	0.2	2	0.004	0	0.01905	0.16	1.82	0.0041	
12	0.2	2	0.002	150	0.01905	0.18	2.05	0.0023	
13	0.7	2	0.002	150	0.0127	0.72	8.18	0.0072	
14	0.7	6	0.002	150	0.0127	1.31	4.96	0.0324	
15	0.45	4	0.002	150	0.0127	0.73	4.15	0.0187	
16	0.2	2	0.004	150	0.0127	0.34	3.86	0.0193	
17	0.7	2	0.004	150	0.0127	0.66	7.5	0.0131	
18	0.2	6	0.002	150	0.01905	0.38	1.44	0.0135	
19	0.7	6	0.004	150	0.01905	1.2	4.55	0.0263	
20	0.45	4	0.004	150	0.01905	0.66	3.75	0.015	
21	0.2	6	0.004	150	0.01905	0.37	1.4	0.0263	
22	0.7	2	0.004	150	0.01905	0.58	6.59	0.0051	

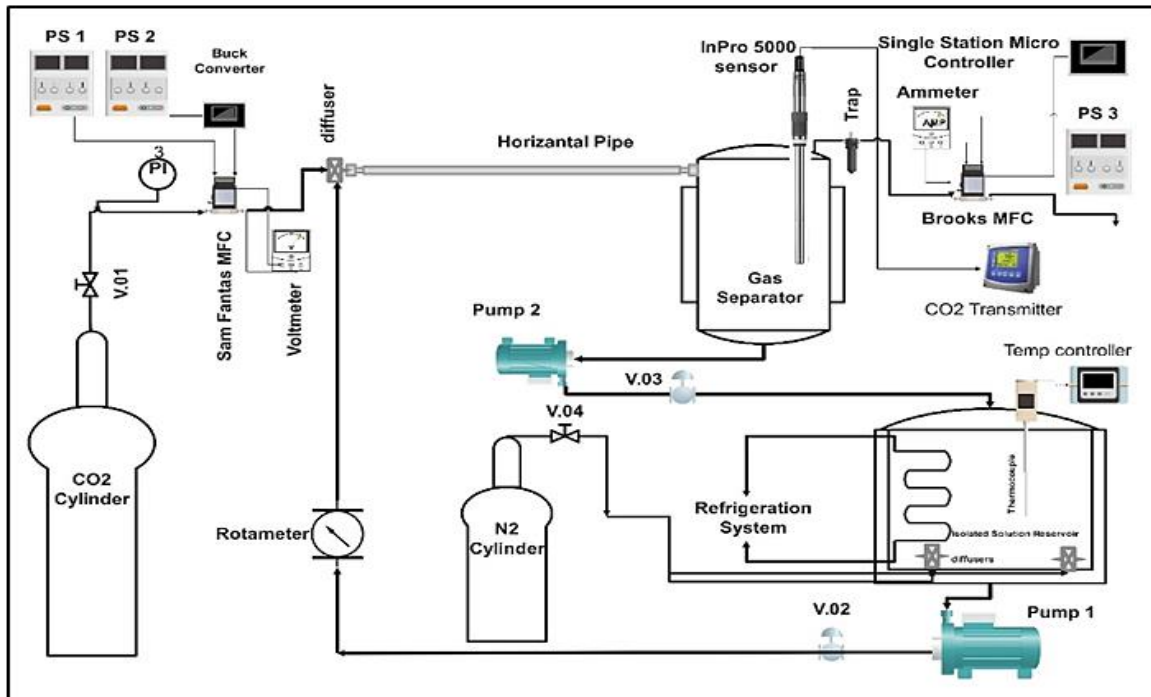


Fig. 1. The schematic setup of two-phase flow horizontal pipe CO₂-sweetener solution study state absorption system

3- Computational model governing equations

The CFD methodology comprises three different steps. The initial step is known as pre-processing, where the geometry and mesh are created, and initial and boundary conditions are specified, along with the selection of physical models. The second stage includes the prescription of solution models, and the final stage is related to the results acquired from the simulation [16]. The interface of two-phase laminar bubbly flow is appropriate for macroscopic modelling of flow consisting of mixtures of liquids and gas bubbles. The second stage includes describing the solution to the mathematical model, and the last stage includes presenting the results.

3.1. Turbulent bubbly flow equation (shear-stress transport (SST) k- ω turbulence models)

The Shear Stress Transfer (SST) k- ω model is a turbulence model developed by Menter as an extension of both the k- ϵ model and the k- ω model [17]. Menter employed the k- ω model near the wall to enhance the accuracy and reliability of the free flow prediction near the wall. The equations governing the turbulent kinetic energy k and specific dissipation rate ω are as follows.

By making the following assumptions, the bubbly flow k- ω model makes the two-fluid concept more satisfactory to understand:

1. The density of a gas is much lower than that of a liquid, so it can be neglected
2. The equilibrium between viscous resistance and pressure forces affects the velocity of the gas bubbles relative to the liquid.
3. The pressure fields of both phases are equal.
4. The environmental conditions in the surrounding area are constant as follows: The temperature is 298 Kelvin and the pressure is 101325 pascals.
5. The gas fed in is an ideal gas. Fluids and gases are both incompressible.
6. The gas bubbles have the same diameter and small size.
7. The temperature of the solution is constant.
8. The surface tension effect is neglected.
9. The physical properties remain constant

By applying these assumptions, the momentum and continuity equations of the two phases combined, while including a gas phase transport equation for measuring the volume fraction of the bubbles. The mathematical equation for momentum is:

$$\phi_l \rho_l \frac{\partial \mathbf{u}_l}{\partial t} + \phi_l \rho_l \mathbf{u}_l \cdot \nabla \mathbf{u}_l = -\nabla p + \nabla \cdot [\phi_l (\mu_l + \mu_T) (\nabla \mathbf{u}_l + \nabla \mathbf{u}_l^T - \frac{2}{3} (\nabla \cdot \mathbf{u}_l) \mathbf{I})] + \phi_l \rho_l \mathbf{g} + \mathbf{F} \quad (3)$$

Where: \mathbf{u}_l is the vector of velocity (m/s), p is the pressure (Pa), ϕ is the phase volume fraction (m³/m³), density (kg/m³), \mathbf{g} is the gravity (m/s²), \mathbf{F} is any additional volume force (N/m³), μ_l is the liquid's dynamic viscosity (Pa·s), μ_T is the turbulent viscosity (Pa·s).

In a description of the liquid phase, the subscript "l" indicates quantities, whereas in the gas phase, the subscript "g" indicates quantities.

In most bubbly flow applications, the flow field behaves with turbulence. To handle this problem, the turbulence $k-\omega$ model has to be employed, and the average velocity field will be estimated. Turbulence occurs because of the motion of gas bubbles and the liquid.

To account for bubble-induced turbulence, the transport equation for the turbulent kinetic energy, k , includes a source term S_k , which is given by:

$$S_k = -C_k \phi_g \nabla p \cdot \mathbf{u}_{slip} \quad (4)$$

The following source term is included in the transport equation for the dissipation rate of turbulent energy, ε :

$$C_\varepsilon S_k \frac{\varepsilon}{k} \quad (5)$$

An additional source term, denoted as ω , is included in the transport equation for the specific dissipation rate.

$$\alpha_\omega S_k \frac{\omega}{k} \quad (6)$$

The values for the model parameters C_k , C_ε , and α_ω are not as well established as single-phase flow parameters. Within the literature, the suggested values for C_k fall

within the range of 0.01 to 1, whereas the range C_ε between 1 and 1.92. α_ω can be defined as:

$$\alpha_\omega = C_\varepsilon - 1 \quad (7)$$

The turbulent viscosity is a term included in the momentum equation, also added when including a drift term in the gas velocity.

$$\mathbf{u}_{drift} = -D_{gc} \frac{\nabla \phi_g}{\phi_g} \quad (8)$$

The stress tensor incorporates an additional contribution, resulting in a modification of the momentum equations, by employing a turbulence model that calculates the turbulent kinetic energy, k , in conjunction with a gas concentration not assumed to be low.

$$\phi_1 \rho_1 \frac{\partial \mathbf{u}_1}{\partial t} + \phi_1 \rho_1 \mathbf{u}_1 \cdot \nabla \mathbf{u}_1 = -\nabla p + \nabla \cdot [\phi_1 (\mu_1 + \mu_T) (\nabla \mathbf{u}_1 + \nabla \mathbf{u}_1^T - \frac{2}{3} (\nabla \cdot \mathbf{u}_1) \mathbf{I}) - \frac{2}{3} \phi_1 \rho_1 k \mathbf{I}] + \phi_1 \rho_1 \mathbf{g} + \mathbf{F} \quad (9)$$

3.2. Transport of diluted species equation

The Transport of Diluted Species interface is used to compute the concentration field of a dilute solute in a solvent. Transport and reactions of the species dissolved in a gas, liquid, or solid can be computed. The driving forces for transport can be diffusion by Fick's law, convection, when coupled to fluid flow, and migration, when coupled to an electric field. Depending on the licensed products, modeling multiple species transport is possible. Also, diffusion, convection, dispersion, adsorption, and volatilization in saturated or partially saturated porous media are available depending on the licensed products. Eq. 10 and Eq. 11 Represent that

$$\nabla \cdot \mathbf{J}_i + \mathbf{u} \cdot \nabla C_i = R_i \quad (10)$$

$$\mathbf{J}_i = -D_i \nabla C_i \quad (11)$$

Where: \mathbf{J}_i is the diffusive flux vector (mol/(m²·s)), R is a production or consumption rate expression (mol/(m³·s)) \mathbf{u} the solvent velocity field (m/s), and D_i diffusion coefficient (m²/s).

3.3. Parameters and boundary conditions

Initially, it is imperative to input all of the parameters and Boundary Conditions to generate the simulation, as illustrated in the following Table 3.

3.4. Geometry and Meshing

The pipe dimensions of length H meter and width W cm were taken for the study, as shown in Fig. 2 COMSOL 5.6 was used for geometry and meshing. The simulation was done using a 2-D model. A Coarse mesh was generated, as shown in Fig. 3. This type was considered the most accurate type for two-phase flow modeling. The description setting of mesh is listed in Table 4 [21-23].

Table 3. Parameters and boundary conditions

Name	Expression	Value	Description
H_CO2	27[L*atm/mol]	2737.8 Pa·m ³ /mol	Henry's constant for CO ₂ in water [18]
k_CO2	0.0002[cm/s]	2E-6 m/s	Mass transfer coefficient of CO ₂ in water [19]
D_CO2	1.401e-9[m ² /s]	3E-9 m ² /s	Diffusion coefficient of CO ₂ [20]
M_CO2	44[g/mol]	0.044 kg/mol	The molecular weight of CO ₂
d	2e-3[m]	0.002 m	Bubble diameter
phig_ini	0	0	Initial gas volume fraction
V_b	4/3*pi*(d/2)^3	4.1888E-9 m ³	Bubble volume
nd_ini	phig_ini/V_b	0 1/m ³	The initial gas number density
rhog_in	1.784[kg/m^3]	1.784 kg/m ³	Density of inlet gas
phig_in	(gfi/(gfi + lf))	0.2	Inlet gas volume fraction
nd_in	phig_in/V_b	4.7746E7 1/m ³	Inlet gas number density
v_in	gfi/A	0.067906 m/s	Inlet gas velocity
W	100[cm]	1 m	width
H	1.25[cm]	0.0125 m	Height
ndf_in	nd_in*vp_in	1.6211E7 1/(m ² .s)	Inlet number density flux
gmf_in	v_in*rhog_in	0.12114 kg/(m ² .s)	Inlet gas mass flux
vp_in	v_in/phig_in	0.33953 m/s	Inlet bubble velocity
A	cross-section	1.2272E-4 m ²	cross-section area
gfi	0.5 [l/min]	8.3333E-6 m ³ /s	gas flow rate inlet
lf	2 [l/min]	3.3333E-5 m ³ /s	liquid flow rate
Uin	lf/A	0.27162 m/s	Inlet liquid velocity
gfo	0.1 [l/min]	1.6667E-6 m ³ /s	gas flow rate out
ndf_out	nd_in*vp_in	1.6211E7 1/(m ² .s)	outnumber density flux
gmf_out	vp_out*rhog_in	0.024229 kg/(m ² .s)	outgas mass flux
vp_out	gfo/A	0.013581 m/s	outlet bubble velocity
phig_out	(gfo/(gfo + lf))	0.047619	outlet gas volume fraction
rhogeff_in	phig_in*rhog_in	0.3568 kg/m ³	Inlet number density
rhogeff_out	phig_out*rhog_in	0.084952 kg/m ³	Inlet number density flux
T	298.15 [K]	298.15 K	Temperature
Us	Uin-v_in	0.10552 m/s	slip velocity

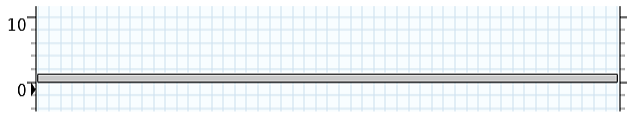


Fig. 2. Geometry horizontal pipe

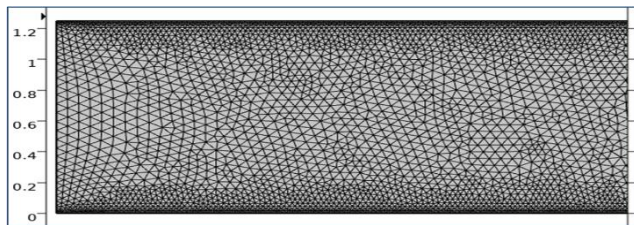


Fig. 3. Mesh horizontal pipe

Table 4. Mesh statics and setting

Description	Value
1 Minimum element quality	0.1595
2 Average element quality	0.7819
3 Triangle	48280
4 Quad	13820
5 Edge element	2818
6 Vertex element	4
Total Element	62100
7 Maximum element size	0.0587
8 Minimum element size	0.00168
9 Curvature factor	0.3
10 Maximum element growth rate	1.13
11 Predefined size	Coarse

3.5. Materials

The solutions used in the simulation were water from the COMSOL library and the sweetener solution, which

consisted of water + 150 g/l sucrose. The sweetener solution was added as a blank material to the COMSOL library, and then the physical properties (density, viscosity, surface tension, and diffusivity) were inserted [20].

4- Results and discussion

COMSOL 5.6 was used in this research to simulate the two-phase flow and mass transfer of CO₂ bubbles in a sweetener solution in a horizontal pipe with bubbly flow k- ω turbulence models.

The CO₂ concentration was determined for the grid independence test by calculating the average concentration of CO₂ in the horizontal pipe of the simulation. The simulation error Table 5 was then estimated as the absolute average relative error between the experimental and simulated CO₂ concentrations.

Table 5. Results of the grid independence test

Mesh	Extremely Coarse	coarser	Coarse	Fine
Total number of cells	16562	45504	69078	283130
Time (min)	3	8	12	115
Concentration	3.69	3.81	3.93	3.94
Simulation error (%)	12.14	9.23	6.42	6.20

As anticipated, the lowest inaccuracy can be obtained by using the Coarse and fine mesh, as the cells in this case have a smaller volume compared to the other case. Since there is very little difference between fine and coarse, coarse was used because the simulation time is much less than fine.

4.1. Comparison with CFD model

The CO₂ concentration was calculated from the experimental run and COMSOL simulation, as well as the simulation error described in Table 6. The simulation

error was calculated as the absolute average relative error between the experimental and simulation CO₂ concentrations.

Table 6. CO₂ concentration experiment, COMSOL CFD results

Run No.	gas flow rate L/min	liquid flow rate L/min	Bubble diameter m	Concentration g/L	pipe diameter m	Experimental CO ₂ Concentration g/m ³	CFD CO ₂ Concentration g/m ³	Error %
1	0.7	2	0.002	0	0.01905	8.07	7.4	8.28
2	0.2	6	0.002	0	0.0127	1.4	1.35	3.68
3	0.2	2	0.002	0	0.0127	3.18	2.9	8.86
4	0.2	6	0.004	0	0.0127	1.17	1.145	2.49
5	0.45	4	0.004	0	0.0127	4.09	3.85	5.89
6	0.7	6	0.004	0	0.0127	4.2	3.93	6.53
7	0.2	2	0.002	0	0.01905	1.59	1.55	2.57
8	0.7	6	0.002	0	0.01905	4.17	4.01	3.76
9	0.45	4	0.002	0	0.01905	3.3	3.21	2.59
10	0.7	2	0.004	0	0.01905	7.5	6.61	11.87
11	0.2	2	0.004	0	0.01905	1.82	1.78	2.1
Total								5.33
12	0.2	2	0.002	150	0.01905	2.05	1.95	4.67
13	0.7	2	0.002	150	0.0127	8.18	7.2	12
14	0.7	6	0.002	150	0.0127	4.96	4.63	6.69
15	0.45	4	0.002	150	0.0127	4.15	3.7	10.79
16	0.2	2	0.004	150	0.0127	3.86	3.4	12
17	0.7	2	0.004	150	0.0127	7.5	6.61	11.87
18	0.2	6	0.002	150	0.01905	1.44	1.35	6.21
19	0.7	6	0.004	150	0.01905	4.55	4.1	9.8
20	0.45	4	0.004	150	0.01905	3.75	3.35	10.67
21	0.2	6	0.004	150	0.01905	1.4	1.3	7.24
22	0.7	2	0.004	150	0.01905	6.59	6.1	7.45
Total								9.47

The error between the simulation and experimental results was 5.33% and 9.47% for the RO water and the sweetener solution (RO water + 150 g/l sucrose), respectively.

4.2. Effect of bubble diameter on concentration distribution and Velocity gas phase

The effect of bubble diameter on the concentration of CO₂ is illustrated in Fig. 4 a, b. In proportion to the decrease in the diameter of the bubble, the concentration of carbon dioxide gas increases because bubbles with a

smaller diameter have a larger contact surface area than bubbles with a larger diameter. Additionally, the mass transfer coefficient increases as the bubble diameter decreases. This is one of the reasons for the increase in CO₂ concentration [24]. Also, the concentration of CO₂ increases with increasing contact time. The contact time for the smaller bubble is greater than the large bubble according to Stoke's law for the velocity of bubbles, which explains the results of Fig. 5 a, b [25]. The concentration and velocity of gas bubbles were measured at the centre of the pipe.

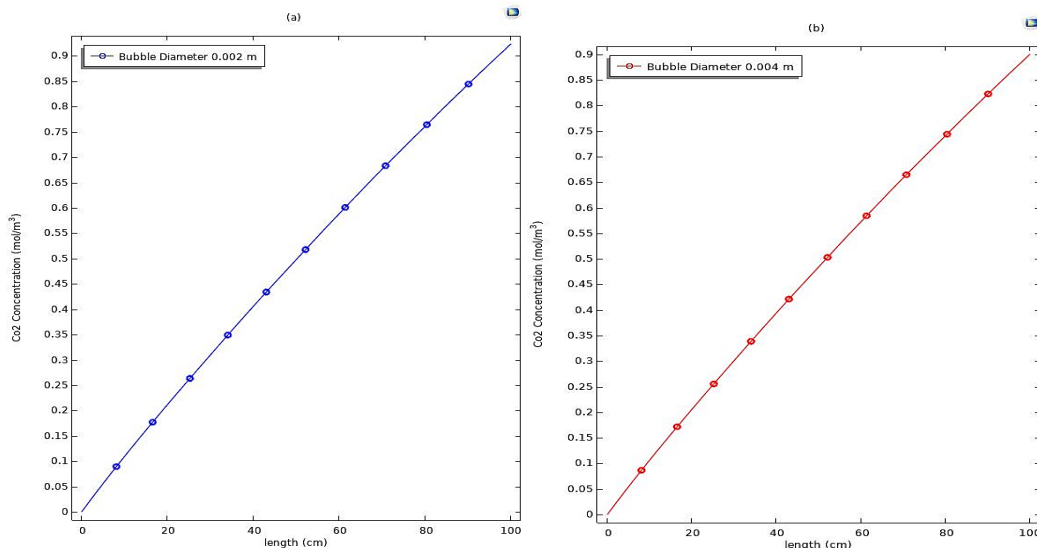


Fig. 4. Effect of bubble diameter on concentration (a) 0.002m, (b) 0.004m

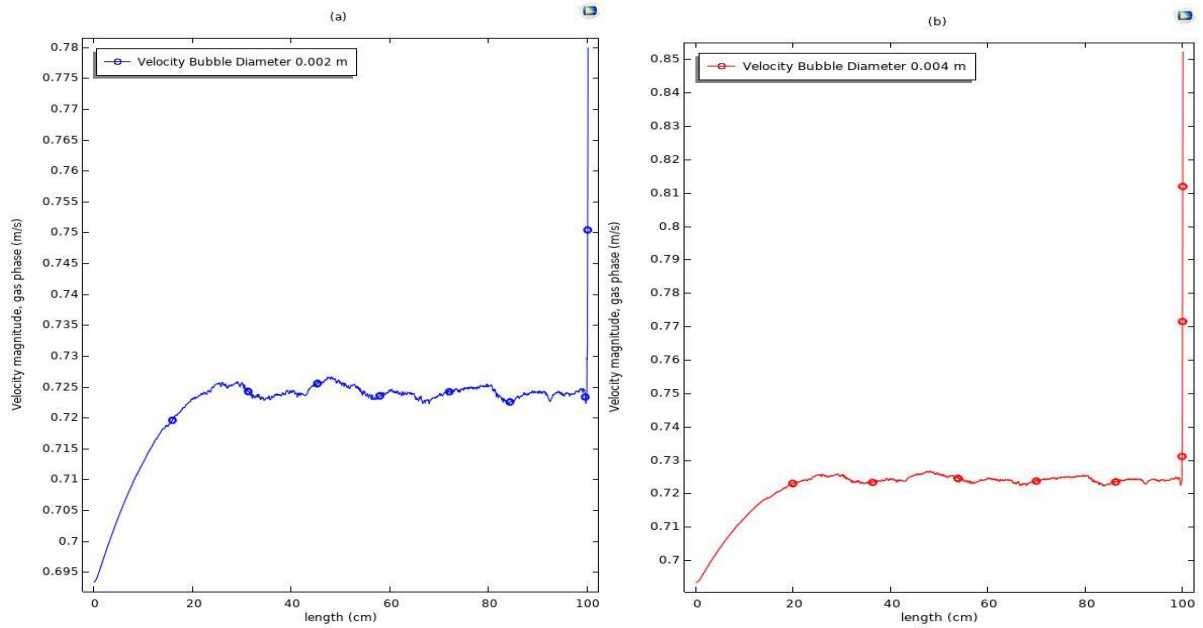


Fig. 5. Effect of bubble diameter on gas phase velocity (a) 0.002m, (b) 0.004m

4.3. Effect of gas and liquid flow rate on concentration distribution

Fig. 6 a, b and Fig. 7 a, b presented the effect of gas and liquid flow rates on the concentration of CO₂. The concentration of CO₂ in the two cases increased with the increase in the flow rate. The increase in the flow rate for both gas and liquid increases the absorption rate of CO₂ gas, accompanied by an increase in the mass transfer coefficient. In addition to increasing the flow rate, the

mixing between the gas and liquid phases increases. As a result, the surface area for absorption increases, and thus the concentration of CO₂ increases [26]. Furthermore, a decrease in the liquid's flow rate improved its capacity to absorb carbon dioxide. In addition to that, the slip velocity affects increasing the CO₂ concentration. The lower the sliding velocity, the greater the absorbed CO₂ concentration. The increased wetting of the gas-liquid interface was a possible explanation for this phenomenon, as shown in Fig. 7 a, b [27].

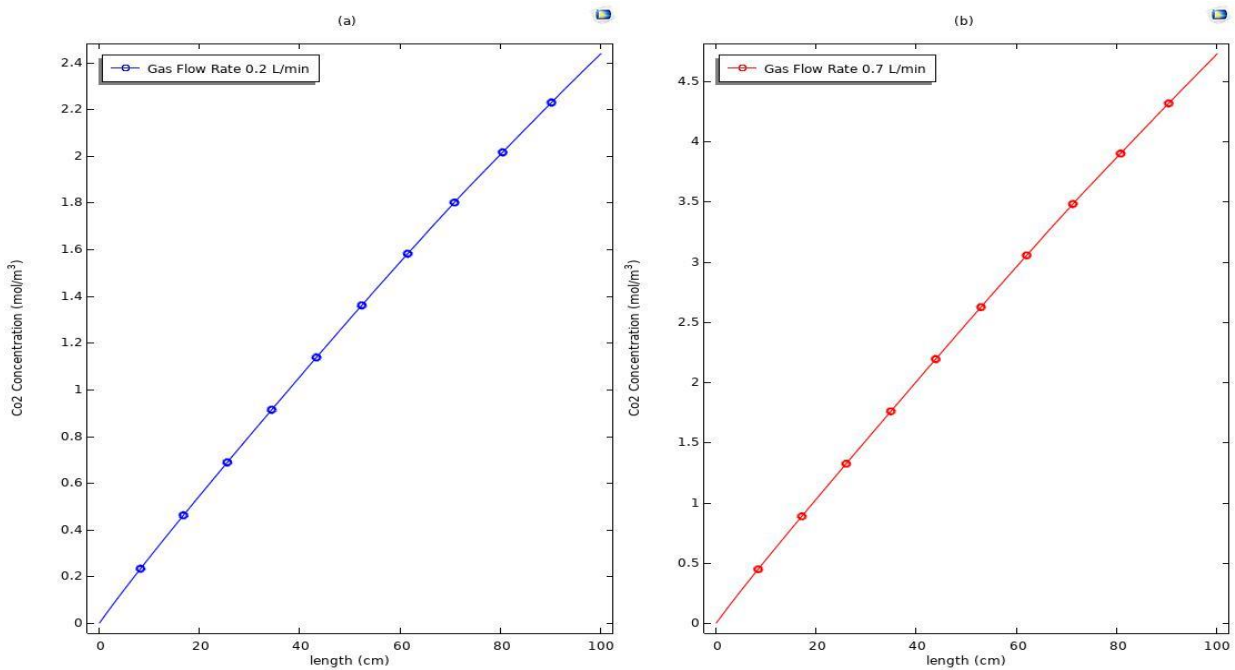


Fig. 6. Effect of gas flow rate on concentration (a) 0.2 L/min, (b) 0.7 L/min

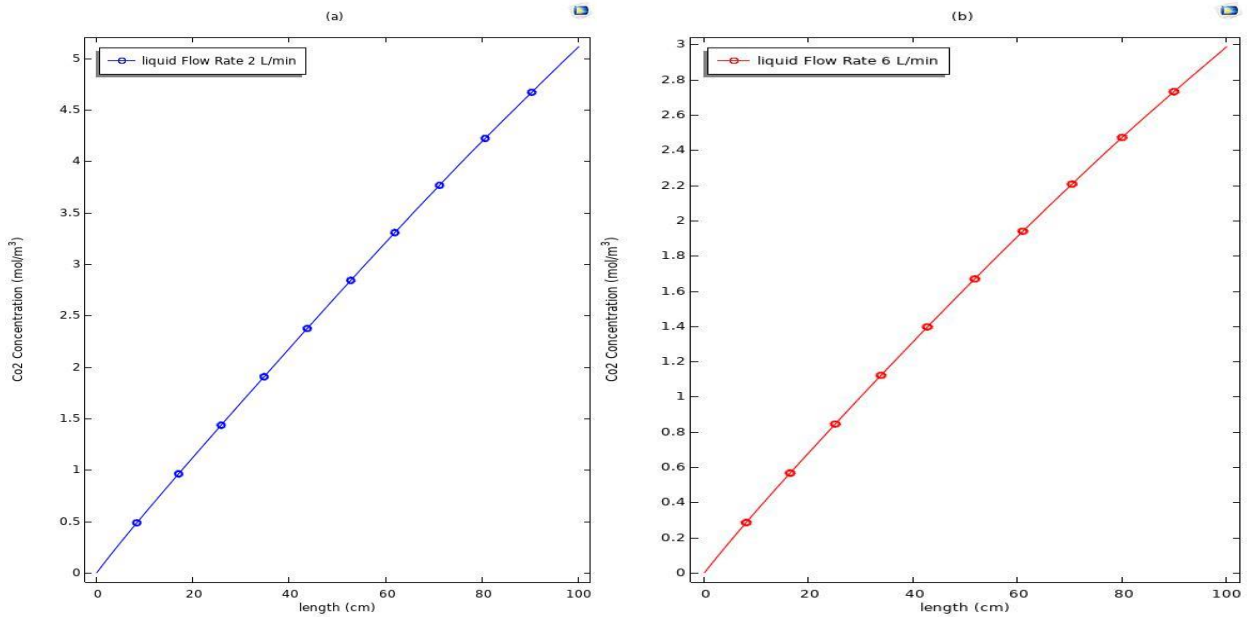


Fig. 7. Effect of liquid flow rate on concentration (a) 2 L/min, (b) 6 L/min

4.4. Effect of the diameter of the pipe on the concentration distribution

Fig. 8 a, b presents the effect of pipe diameter on the concentration of CO₂. The relationship between the pipe

diameter and the concentration of dissolved CO₂ is indirect, as the diameter of the pipe reduces, the concentration of CO₂ increases due to an increase in the mass transfer coefficient [28].

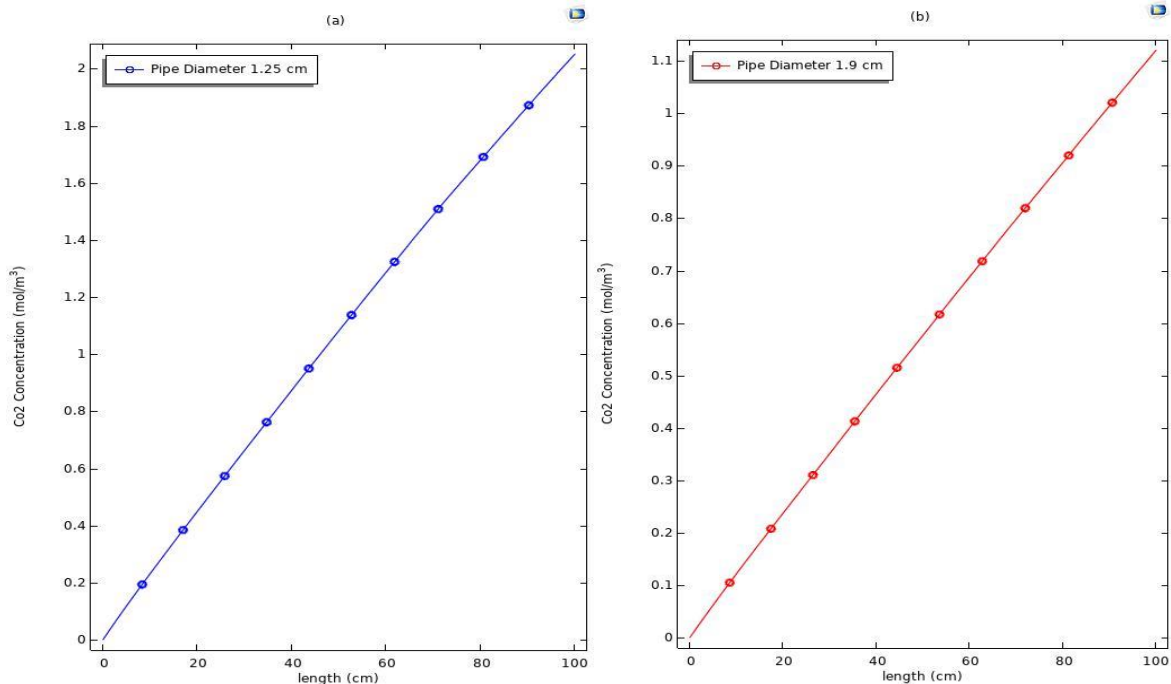


Fig. 8. Effect of pipe diameter on concentration (a) 1.25 cm, (b) 1.9 cm

4.5. Effect of type of material on the concentration distribution

Fig. 9 a, b illustrates the effects of material type and its properties on the absorption of carbon dioxide gas. The increase in carbon dioxide gas absorption with decreased

sugar concentration and decreased diffusivity is due to changes in the physical properties of the solution, including increased density, viscosity, and surface tension [29].

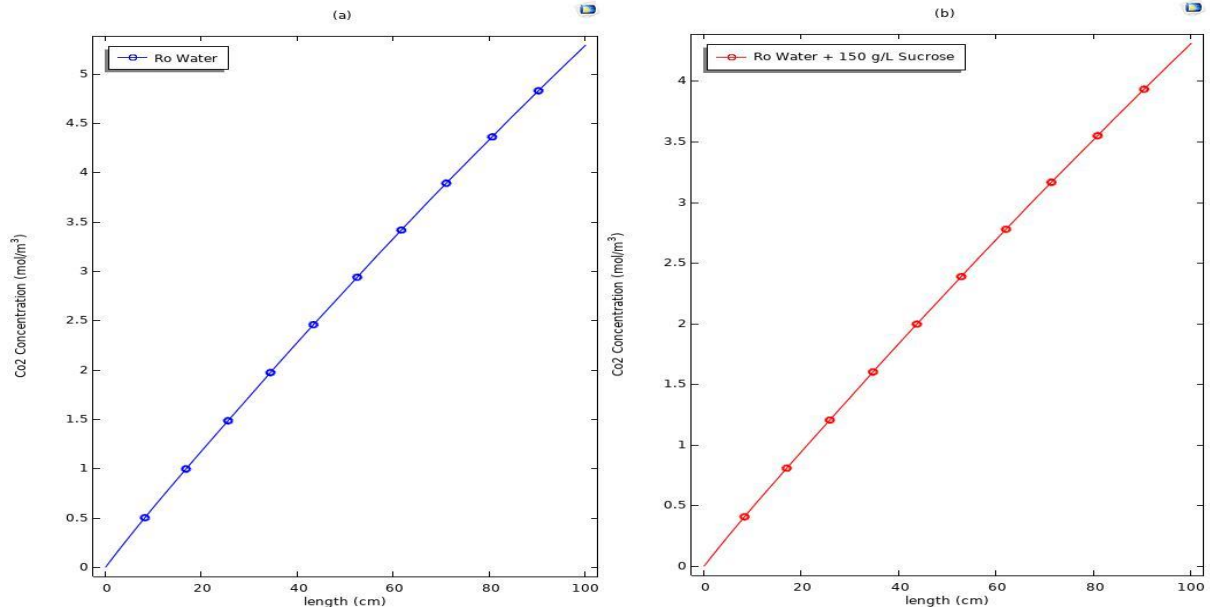


Fig. 9. Effect of type of material on concentration (a) Ro water, (b) Ro water + 150 g/L sucrose

4.6. Share rate distribution

Fig. 10 a, b clearly shows the relationship between the shear distribution rate and the pipe diameter. The

relationship between them was an inverse relationship. The highest rate of shear distribution was at the smallest pipe (diameter). A decrease in the pressure drop inside the pipe leads to an increase in the shear rate [30].

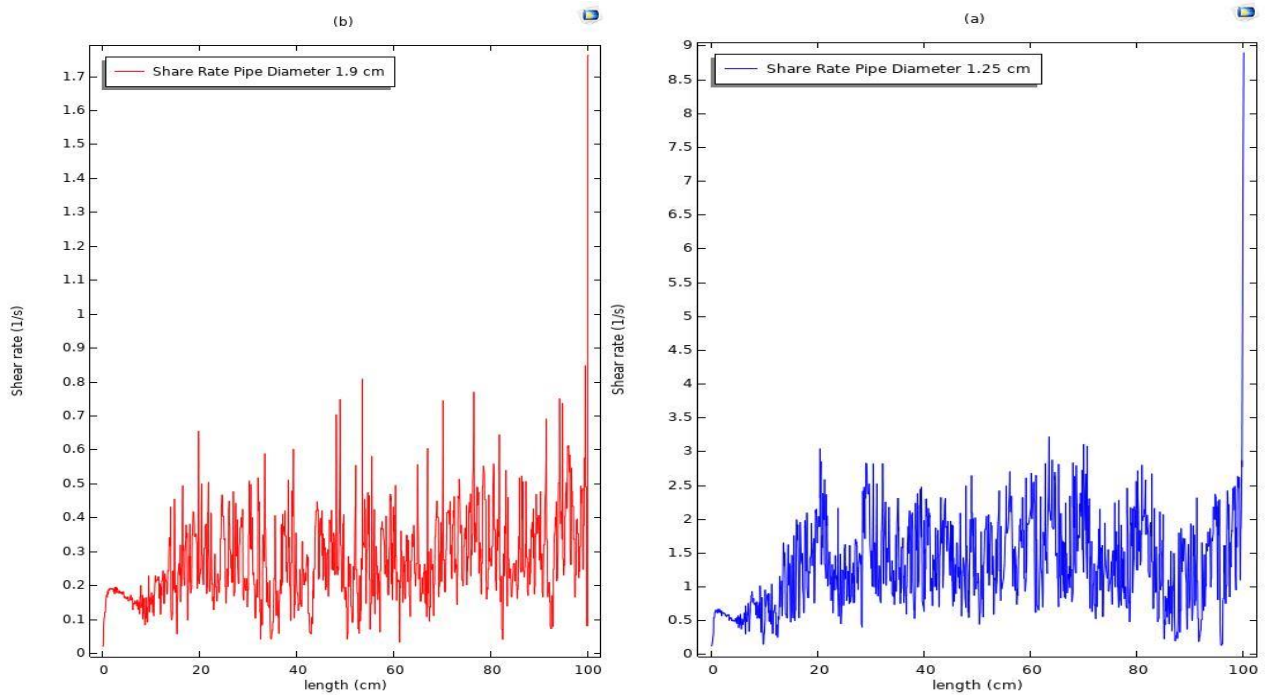


Fig. 10. Effect of pipe diameter on share rate (a) 1.25 cm, (b) 1.9 cm

Fig. 11 a, b shows the relationship between the shear distribution rate and the bubble diameter. The figure shows that there is a slight effect of increasing the share rate by increasing the size of the bubble.

Fig. 12 a, b shows the relationship between the shear distribution rate and liquid flow rate. The figure shows

that there is a high effect of increasing the share rate by increasing the Liquid flow rate. Fig. 13 a, b shows the relationship between the shear distribution rate and gas flow rate. The relationship between them was an inverse relationship [30]

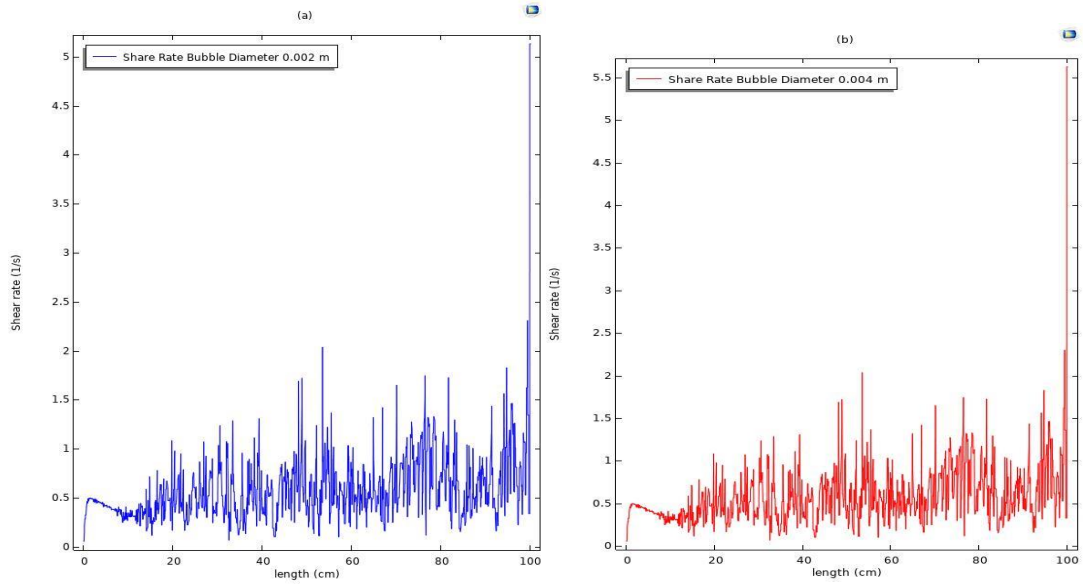


Fig. 11. Effect of bubble diameter on share rate(a) 0.002m, (b) 0.004m

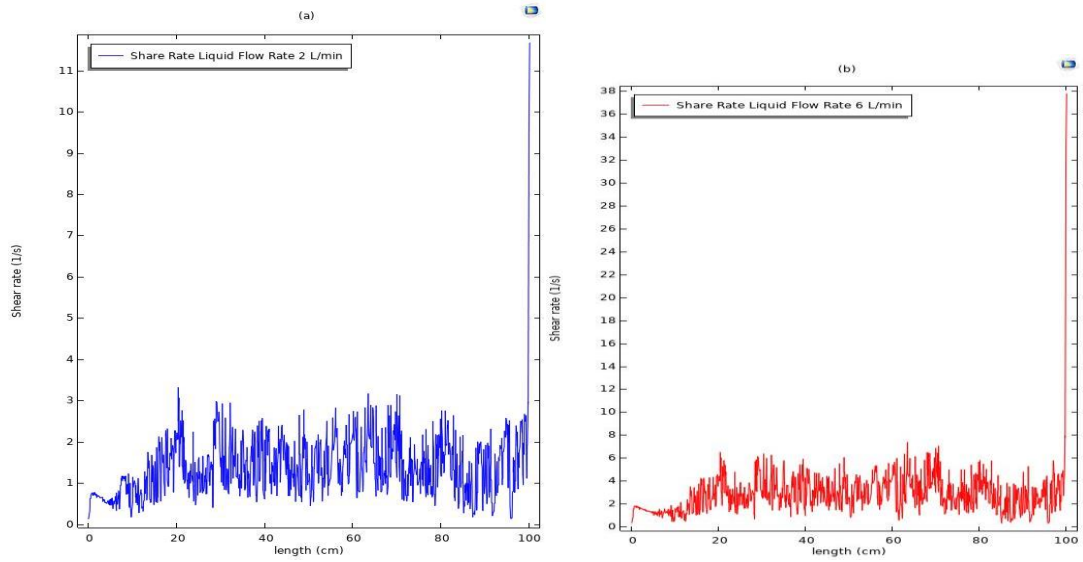


Fig. 12. Effect of liquid flow rate on share rate (a) 2 L/min, (b) 6 L/min

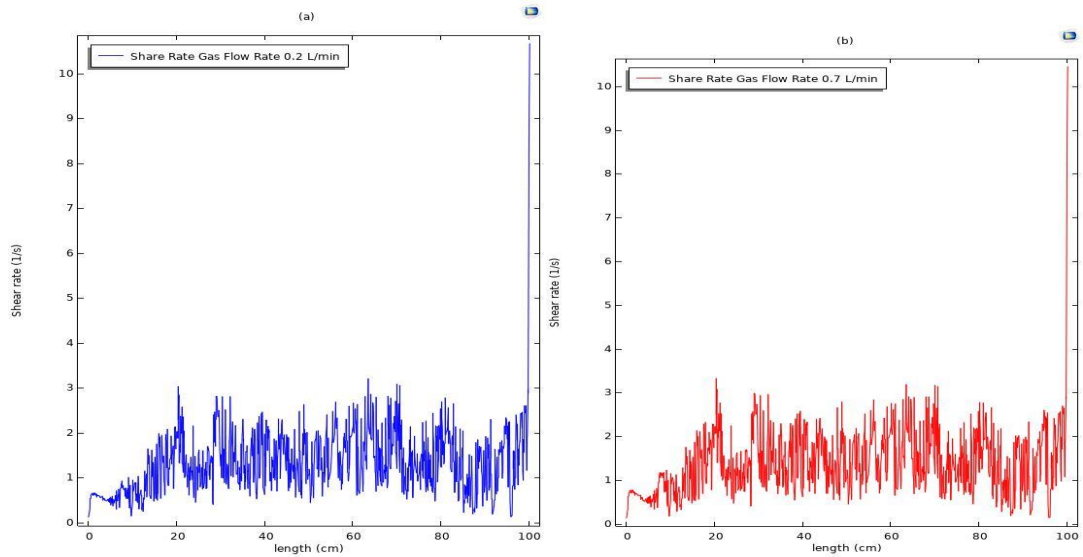


Fig. 13. Effect of gas flow rate on share rate (a) 0.2 L/min, (b) 0.7 L/min

5- Conclusion

The simulation of a two-phase flow, including a sweetened solution with CO₂, was carried out using the COMSOL software and compared with experimental results. The modeling of the bubble flow k- ω turbulence models with the mass transfer was based on the computational fluid dynamics (CFD) method. According to the report extracted from the COMSOL programmer, it was found the error between the simulation and experimental results was 5.33% for the RO water, while for the sweetener solution (RO water + 150 g/l sucrose), it was 9.47% by using a Coarse mesh the CFD model demonstrated satisfactory concurrence with the experimental data. Also, the effect of bubble size and pipe diameter on increasing CO₂ concentration was inverse, while the flow rate of gas and liquid had increased together. The concentration of CO₂ decreases as the concentration of sucrose increases. The relationship between bubble diameter and gas phase velocity was inverse. The report showed the effect of variables on share rate distribution during the process.

References

- [1] D. Kregiel, "Health safety of soft drinks: contents, containers, and microorganisms," *BioMed Research International*, vol. 2015, 2015, pp. 1–15. <https://doi.org/10.1155/2015/128697>
- [2] G. Kocamustafaogullari and W. D. Huang, "Internal structure and interfacial velocity development for bubbly two-phase flow," *Nuclear engineering and design*, vol. 151, no. 1, 1994, pp. 79–101. [https://doi.org/10.1016/0029-5493\(94\)90035-3](https://doi.org/10.1016/0029-5493(94)90035-3)
- [3] A. B. Desamala, A. K. Dasamahapatra, and T. K. Mandal, "Oil-water two-phase flow characteristics in horizontal pipeline—a comprehensive CFD study," *International journal of Chemical, Molecular, Nuclear, Materials and Metallurgical Engineering, World Academy of Science, Engineering and Technology*, vol. 8, no. 4, 2014, pp. 360–364.
- [4] M. E. Nakhchi and J. A. Esfahani, "CFD approach for two-phase CuO nanofluid flow through heat exchangers enhanced by double perforated louvered strip insert," *Powder Technology*, vol. 367, 2020, pp. 877–888. <https://doi.org/10.1016/j.powtec.2020.04.043>
- [5] A. Boemer, H. Qi, and U. Renz, "Eulerian simulation of bubble formation at a jet in a two-dimensional fluidized bed," *International Journal of Multiphase Flow*, vol. 23, 1997, pp. 927–944. [https://doi.org/10.1016/s0301-9322\(97\)00018-9](https://doi.org/10.1016/s0301-9322(97)00018-9)
- [6] M. H. Zawawi, M. G. Swee, N. S. Zainal, N. M. Zahari, M. A. Kamarudin, and M. Z. Ramli, "Computational fluid dynamic analysis for independent floating water treatment device," in *AIP Conference Proceedings*, 2017. <https://doi.org/10.1063/1.5002316>
- [7] J. Parekh and R. Rzehak, "Euler–Euler multiphase CFD-simulation with full Reynolds stress model and anisotropic bubble-induced turbulence," *International Journal of Multiphase Flow*, vol. 99, 2018, pp. 231–245. <https://doi.org/10.1016/j.ijmultiphaseflow.2017.10.012>
- [8] Z. Yang, "On modeling of CO₂ two-phase flow in a near horizontal pipe," in *Proceedings of the 16th Greenhouse Gas Control Technologies Conference (GHGT-16)* 23-24 Oct, 2022. <https://doi.org/10.2139/ssrn.4274197>
- [9] R. A. Mahmood, D. Buttsworth, R. Malpress, and A. Sharifian-Barforoush, "CFD numerical and experimental investigation of two-phase flow development after an expansion device in a horizontal pipe," *Journal of Thermal Engineering*, vol. 7, no. 1, 2021, pp. 307–323. <https://doi.org/10.18186/thermal.850672>
- [10] U. Khan, W. Pao, N. Sallih, and F. Hassan, "Identification of horizontal gas-liquid two-phase flow regime using deep learning," *CFD Letters*, vol. 14, no. 10, 2022, pp. 68–78. <https://doi.org/10.37934/cfdl.14.10.6878>
- [11] G. Kocamustafaogullari and Z. Wang, "An experimental study on local interfacial parameters in a horizontal bubbly two-phase flow," *International journal of multiphase flow*, vol. 17, no. 5, 1991, pp. 553–572. [https://doi.org/10.1016/0301-9322\(91\)90024-w](https://doi.org/10.1016/0301-9322(91)90024-w)
- [12] G. Kocamustafaogullari and W. D. Huang, "Internal structure and interfacial velocity development for bubbly two-phase flow," *Nuclear engineering and design*, vol. 151, no. 1, 1994, pp. 79–101. [https://doi.org/10.1016/0029-5493\(94\)90035-3](https://doi.org/10.1016/0029-5493(94)90035-3)
- [13] R. Maceiras, X. R. Nóvoa, E. Alvarez, and M. A. Cancela, "Local mass transfer measurements in a bubble column using an electrochemical technique," *Chemical Engineering and Processing-Process Intensification*, vol. 46, no. 10, 2007, pp. 1006–1011. <https://doi.org/10.1016/j.cep.2007.05.010>
- [14] K. Ekambara, R. S. Sanders, K. Nandakumar, and J. H. Masliyah, "CFD simulation of bubbly two-phase flow in horizontal pipes," *Chemical Engineering Journal*, vol. 144, no. 2, 2008, pp. 277–288. <https://doi.org/10.1016/j.cej.2008.06.008>
- [15] J. E. Olsen, D. Dunnebie, E. Davies, P. Skjetne, and J. Morud, "Mass transfer between bubbles and seawater," *Chemical Engineering Science*, vol. 161, 2017, pp. 308–315. <https://doi.org/10.1016/j.ces.2016.12.047>
- [16] A. F. Melo Zambrano and N. Ratkovich, "CFD modeling of Air-Water Two-phase Annular Flow before a 90° elbow," *Revista De Ingenieria*, no. 43, 2015, pp. 16–23. <https://doi.org/10.16924/riua.v0i43.843>

- [17] F. R. Menter, "Two-equation eddy-viscosity turbulence models for engineering applications," *American Institute of Aeronautics and Astronautics Journal*, vol. 32, no. 8, 1994, pp. 1598–1605. <https://doi.org/10.2514/3.12149>
- [18] J. J. Carroll, J. D. Slupsky, and A. E. Mather, "The solubility of carbon dioxide in water at low pressure," *Journal of Physical and Chemical Reference Data*, vol. 20, no. 6, 1991, pp. 1201–1209. <https://doi.org/10.1063/1.555900>
- [19] C. W. Bowman and A. I. Johnson, "Mass transfer from carbon dioxide bubbles rising in water," *Canadian Journal of Chemical Engineering*, vol. 40, no. 4, 1962, pp. 139–147. <https://doi.org/10.1002/cjce.5450400404>
- [20] E. Alvarez, M. A. Cancela, J. M. Navaza, and R. Taboas, "Mass transfer coefficients in batch and continuous regime in a bubble column," in *Proceedings International Conference on Distillation & Absorption*, 2002.
- [21] Y. Wen, Z. Wu, J. Wang, J. Wu, Q. Yin, and W. Luo, "Experimental study of liquid holdup of liquid-gas two-phase flow in horizontal and inclined pipes," *Heat and Technology*, vol. 35, no. 4, 2017, pp. 713–720. <https://doi.org/10.18280/jht.350404>
- [22] M. Abdulkadir, V. Hernandez-Perez, S. Lo, I. S. Lowndes, and B. J. Azzopardi, "Comparison of experimental and computational fluid dynamics (CFD) studies of slug flow in a vertical 90 bend," *The Journal of Computational Multiphase Flows*, vol. 5, no. 4, 2013, pp. 265–281. <https://doi.org/10.1260/1757-482x.5.4.265>
- [23] V. Hernandez-Perez, M. Abdulkadir, and B. J. Azzopardi, "Grid generation issues in the CFD modelling of two-phase flow in a pipe," *The Journal of Computational Multiphase Flows*, vol. 3, no. 1, 2011, pp. 13–26. <https://doi.org/10.1260/1757-482x.3.1.13>
- [24] H.-J. Cho and J. Choi, "Calculation of the Mass Transfer Coefficient for the Dissolution of Multiple Carbon Dioxide Bubbles in Sea Water under Varying Conditions," *Journal of Marine Science and Engineering*, vol. 7, no. 12, 2019, p. 457. <https://doi.org/10.3390/jmse7120457>
- [25] N. M. Aybers and A. Tapucu, "The motion of gas bubbles rising through stagnant liquid," *Wärme-und Stoffübertragung*, vol. 2, 1969, pp. 118–128. <https://doi.org/10.1007/bf01089056>
- [26] M. Tokumura, M. Baba, and Y. Kawase, "Dynamic modeling and simulation of absorption of carbon dioxide into seawater," *Chemical Engineering Science*, vol. 62, no. 24, 2007, pp. 7305–7311. <https://doi.org/10.1016/j.ces.2007.08.074>
- [27] A. Aroonwilas, A. Veawab, and P. Tontiwachwuthikul, "Behavior of the mass-transfer coefficient of structured packings in CO₂ absorbers with chemical reactions," *Industrial & Engineering Chemistry Research*, vol. 38, no. 5, 1999, pp. 2044–2050. <https://doi.org/10.1021/ie980728c>
- [28] A. K. Thandlam, C. Das, and S. K. Majumder, "Flow pattern-based mass and heat transfer and frictional drag of gas-non-Newtonian liquid flow in helical coil: two-and three-phase systems," *Heat and Mass transfer*, vol. 53, 2017, pp. 1183–1197. <https://doi.org/10.1007/s00231-016-1898-y>
- [29] C. Descoins, M. Mathlouthi, M. Le Moual, and J. Hennequin, "Carbonation monitoring of beverage in a laboratory scale unit with on-line measurement of dissolved CO₂," *Food Chemistry*, vol. 95, no. 4, 2006, pp. 541–553. <https://doi.org/10.1016/j.foodchem.2004.11.031>
- [30] W. A. Noori, D. A. H. AlTimimi, and B. J. Kadhim, "Simulation of Two-Phase Flow Mixing Co-Current in T Junction Using Comsol," *Iraqi Journal of Chemical and Petroleum Engineering*, vol. 21, no. 1, 2020, pp. 67–74. <https://doi.org/10.31699/ijcpe.2020.1.10>

محاكاة عملية جريان ثنائي الطور مع انتقال كتلة لفقاعات ثنائي اوكسيد الكربون في محلول محلي في انبوب افقي باستخدام برنامج كومسول

احمد ضياء نصيف^{١*}، ابتهال كريم شاكر^١، مناف اللامي^٢

^١ قسم الهندسة الكيميائية، كلية الهندسة، جامعة بغداد، بغداد، العراق

^٢ قسم الهندسة الكيميائية والبيئية، كلية التكنولوجيا الكيميائية والتكنولوجيا الحيوية، جامعة بوابست للتكنولوجيا والاقتصاد، بوابست، هنجاريا

الخلاصة

تم إجراء دراسة سلوك التدفق ثنائي الطور، وانتقال فقاعات ثاني أكسيد الكربون في محلول الماء والسكر في الأنابيب الأفقية باستخدام نموذج ديناميكي الموائع الحسابي (CFD) الذي يحتوي على أقسام تطبيقية في صناعات مختلفة. تم إجراء محاكاة التدفق ثنائي الطور مع النقل الجماعي باستخدام برنامج COMSOL بالإصدار ٥,٦ ومقارنته بالنتائج العملية و دراسة المتغيرات المتعددة مثل التركيز والسرعة ومعدل الاجهاد بمتغيرات مختلفة (معدل تدفق الغاز، معدل تدفق السائل، قطر الفقاعة، قطر الأنبوب، تركيز السكر). تباين معدل سريان الغاز و كانت القيم (٠,٢، ٠,٤٥، ٠,٧ لتر/دقيقة) لثاني اوكسيد الكربون، و (٢، ٤، ٦ لتر/دقيقة) للمحلول المحلي. تراوحت أقطار الفقاعات بين (٢ و ٤ ملم) وكان قطر الأنبوب (١,٢٥، ١,٩، ١,٩ سم) بينما تركيز السكر في محلول المحلي ١٥٠ جم/لتر. وقد لوحظ أن تأثير قطر الفقاعة كان عكسيا مع تركيز ثاني اوكسيد الكربون، كما أن معدلات تدفق الغاز والسائل تتناسب طرديا مع التركيز. وكانت العلاقة بين قطر الفقاعة وسرعة الطور الغازي علاقة عكسية. وقل تركيز CO₂ مع زيادة تركيز السكر وكذلك دراسة تأثير المتغيرات على معدل القص.

الكلمات الدالة: جريان ثنائي الطور، برنامج كومسول، انتقال كتلة، فقاعات ثنائي اوكسيد الكربون، انبوب افقي.